

Article

Evaporation-Induced Crystal Nucleation and Morphology of Dried Poly(Vinylidene Fluoride) Droplets

Yongri Liang ^{1,2,*}  and Susu Wang ²

¹ State Key Lab of Metastable Materials Science and Technology, School of Materials Science and Engineering, Yanshan University, No. 438 West Hebei Avenue, Qinhuangdao 066004, China

² College of Materials Science and Engineering, Beijing Institute of Petrochemical Technology, Beijing 102617, China; wangsusu@bjfleming.com

* Correspondence: liangyr@ysu.edu.cn; Tel.: +86-18010156705

Abstract: The evaporation of a polymer solution droplet is important in solution-based polymer film fabrications, such as inkjet printing, spray coatings, and droplet casting, etc. In this work, we investigated the effect of droplet size, solvent evaporation rate, and concentration on the “coffee-ring” effect, crystal nucleation, polymorphism, and morphology of dried poly(vinylidene fluoride) (PVDF) solution droplets with the atomic force microscopy (AFM) and two-dimensional grazing incidence wide angle X-ray scattering (2D GIWAXS) method. We found that the crystal structure, morphology and crystal distribution in the center and edge regions of dried PVDF droplets were different due to the “coffee-ring” effect. The “coffee-ring” effect of dried PVDF droplets was mainly composed of accumulated crystals at the edge region of a droplet, which was mainly made by the crystallization of migrated chains. The interplay between the migration of chains and the crystallization and solidification of PVDF droplets significantly influenced the formation of the “coffee-ring”. In addition, our results showed that the decrease in droplet size and the controlling solvent evaporation rate were effective ways to improve the electroactive crystalline phases (β and γ -phases) nucleation and decrease the crystal size.

Keywords: evaporation; poly(vinylidene fluoride); crystallization; droplet; coffee ring effect; ultrasonic spray



Citation: Liang, Y.; Wang, S. Evaporation-Induced Crystal Nucleation and Morphology of Dried Poly(Vinylidene Fluoride) Droplets. *Crystals* **2021**, *11*, 1442. <https://doi.org/10.3390/cryst11121442>

Academic Editors: Günter Reiter, Jun Xu, Rufina G. Alamo and Andrónico Neira-Carrillo

Received: 26 October 2021
Accepted: 22 November 2021
Published: 23 November 2021

Publisher’s Note: MDPI stays neutral with regard to jurisdictional claims in published maps and institutional affiliations.



Copyright: © 2021 by the authors. Licensee MDPI, Basel, Switzerland. This article is an open access article distributed under the terms and conditions of the Creative Commons Attribution (CC BY) license (<https://creativecommons.org/licenses/by/4.0/>).

1. Introduction

The evaporation of polymer solution droplets is very important in some solution-based polymer film fabrications, such as inkjet printing, spray coatings, and droplet casting, etc. [1]. The evaporation process of polymer solution droplets is a very complex non-equilibrium process, where many factors influence the final morphology and structure of the dried polymer solution droplets, such as the evaporation rate, diffusion rate of solute, and phase transition, etc. [2]. In contrast with solution casting and blade coating processes, the evaporation of droplets generally generates a “coffee-ring” effect that generally occurs by an evaporation-induced outward capillary flow [3–7]. Therefore, understanding the interplay between the solvent evaporation and the crystallization of polymer solution droplets is very important to control the final morphology of dried polymer solution droplets and droplet-deposited polymer films.

In the droplet evaporation, the capillary outward flow will be induced inside the pinned droplet and can carry almost all the dispersed solute to the edge to form a ring-like deposit, i.e., pinning the drop at triple-phase contact lines (TPCL) along with faster evaporation leads to the defined ring structure. In addition, a concentration driven surface tension gradient leads to a Marangoni flow that drives the solution in a path opposite to the outward capillary flow [3]. Therefore, there is a competition between capillary convection and the solute Marangoni flow and only a weak Marangoni flow of the solution can create a “coffee-ring”. Recently, Hu et al. [8] investigated the “spherulites ring” morphology and

“coffee-ring” profile of a polyethylene oxide (PEO) film formed by drying the droplet at a glass substrate with a different heating rate. They found that the outward capillary flow is the dominant micro-flow inside the drying droplet of a PEO aqueous solution when the substrate temperature is below 50 °C. The solute is carried by the capillary flow to the edge of the droplet and forms the profile of a “coffee-ring”. The spherulites come together in the center of the PEO film. Marangoni convection carries much solute to the middle of droplets when the substrate temperature is above 70 °C and forms the regular “spherulites ring” at the position of the Marangoni convection center. Rietveld et al. [9] investigated the effect of the electrospray process on the morphology of PVDF films. They suggested that the droplet size of the spray and the viscosity of the solution at deposition are the two main factors determining the morphology of the PVDF film, and the solvent is the key parameter to produce polymer thin films in the electrospray process. More recently, we found that a high β -phase content and the high transparency of poly(vinylidene fluoride) (PVDF) film can be achieved using the ultrasonic spray coating (USC) method [10]. In contrast with the conventional blade coating process, the evaporation-induced outward capillary flow can play an important role in the nucleation of PVDF β -phase in the USC process due to fast solvent evaporation. However, as far as we know, the evaporation-induced crystal nucleation and the morphology of polymer solution droplets has not been fully understood thus far.

In this work, we prepared various sizes of PVDF solution droplets using dropping and USC methods, and investigated the effect of droplet size, solvent evaporation rate and concentration on the crystal nucleation and morphology of dried PVDF droplets with the atomic force microscopy (AFM) method. The crystal structure and morphology of ultrasonic spray-coated PVDF films were also investigated.

2. Materials and Methods

PVDF ($M_w \approx 534,000$) was purchased from Sigma-Aldrich Co., Ltd. (Shanghai, China). The Indium tin oxide (ITO) glasses with 6 Ω of resistivity were purchased from Beijing Zhenyongwei Technology Co., Ltd. (Beijing, China). The ethyl alcohol, acetone (AC), and N,N-dimethylformamide (DMF) were purchased from Beijing Chemical Works (Beijing, China). Additionally, all the chemicals were analytical reagent, and were used without further purification.

The PVDF powders were dissolved in a selected solvent at 70 °C for 4 h for preparation of the PVDF solutions with 12 mg/ml of concentration. The ITO glasses were used as a substrate for drying the PVDF solution droplets. The ITO glasses were cleaned in deionized water and ethyl alcohol for 5 min in an ultrasonic bath in turn. The washed ITO glasses were dried using nitrogen gas, and then were treated with plasma for 3 min before use. Large size (L) droplets of PVDF solution, a few millimeters in diameter, were prepared by dropping 2 μ L of PVDF solution using 5 mL of a syringe, and they were dried at room temperature. The tens micrometers diameter of PVDF solution small size (S) droplets were prepared using the ultrasonic spray method [10] at room temperature or 70 °C. The height of ultrasonic nozzle (Siansonic Technology Co., Ltd., Beijing, China) from substrate was 15 cm for an ultrasonic spray coating with 1 W of the power.

The ultrasonic spray coated PVDF films were prepared using 12 mg/mL of concentration with a mixed solvent of DMA/AC (6/4 v/v). The ITO-coated glasses were used as a substrate for coating PVDF films. The ITO-coated glasses were cleaned in deionized water and ethyl alcohol for 5 min in an ultrasonic bath in turn, and then were dried using nitrogen gas, and then were treated by plasma for 3 min before use. The height of ultrasonic nozzle from substrate was 15 cm and the flow rate for ultrasonic spray coating with 1 W of the power was 0.1 mL/min.

The morphology of dried PVDF films were characterized using atomic force microscopy (AFM) in MFP-3D Origin AFM system (Oxford Instruments Co. Ltd., Concord, MA, USA), and optical microscopy (OM) (LV100ND, Nikon Co. Ltd., Tokyo, Japan). The AFM tips (AC240TS-R3, Asylum Research, Santa Barbara, CA, USA) with 2 N/m spring

constant and 70 kHz of resonance frequency were used for measurements. The Fourier transform infrared spectroscopy (FTIR) measurements were carried out in FTIR-850 Fourier transform infrared spectrometer (TIANJIN GANGDONG Co. Ltd., Tianjin, China) with transmission mode using 4 cm^{-1} of resolution and 32 scan times.

The crystal structure of ultrasonic spray coated PVDF films were characterized using the two-dimensional grazing incidence wide angle X-ray scattering (2D GIWAXS) method. In the Beijing Synchrotron Radiation Facility (BSRF, Beijing, China), 2D GIWAXS measurements were performed at room temperature on 1W1A Beamline, with a wavelength of 1.54816 \AA and using a Mar345 (3450×3450 pixels, pixel distance: $100\text{ }\mu\text{m}$) detector. Silver behenate ($d_{001} = 58.380\text{ \AA}$) powder was used as standard material to calibrate the scattering angle. The incident angle, α_i was set as 0.2° and the exposure time was 480 s. The air scattering was subtracted before analysis of all 2D GIWAXS patterns.

3. Results

3.1. Solvent Evaporation Induced Crystal Nucleation and Morphology of PVDF/DMF Solution Large Size Droplet

To investigate the effect of droplet size on PVDF nucleation and morphology, we prepared L and S sizes of the PVDF/DMF solution drops with DMF solvent. Figure 1 shows an OM and an AFM image of a partially dried PVDF/DMF solution L-droplet, respectively. The OM image of the dried PVDF/DMF solution L-droplet showed it to be about 5.03 mm in diameter. Additionally, the crystals presented in the edge region of the PVDF L-droplet is denser than that in center region. It indicates that the evaporation of the L-droplet can form the “coffee-ring” effect. The “coffee-ring” effect generally occurs at triple-phase contact lines (TPCL) in the case of the evaporation of droplets due to an outward capillary flow [3,5].

The crystals in the edge region of the dried PVDF/DMF solution L-droplet showed an area a few micrometers in size of particle-like crystals, which have a hill-like shaped morphology and smooth surface (Figure 1F), and had accumulated together. (Figure 1C,D), whereas the crystals in the center region of the dried PVDF/DMF solution L-droplet exhibited a jigsaw-puzzle-like structure, pieced together with remarkable boundaries (Figure 2). This means that the PVDF crystals in the center region collided after crystal growth, which is different to the situation of the accumulated crystals in the edge region, i.e., the mechanism of crystal nucleation and the growth of PVDF in center region is different to that in the edge region. Since the evaporation rate in the edge region is faster than that in center region, the crystal nucleation and growth in edge region should be more constrained by the fast evaporation-caused solidification. In addition, the evaporation-induced outward capillary flow can influence the accumulation of polymer coils and crystals. For the crystal accumulation in the dried L-droplet edge region, two possible mechanisms may be possible. One possibility is that the crystal nuclei are formed in the edge region, and the crystal growth is limited by fast evaporation-induced solidification. In that case, the polymer chains may have migrated from the center region to the edge region of the droplet by evaporation-induced outward capillary flow before crystallization. The other possibility is that the crystal nuclei are formed at a certain center region, and then the small sized crystals are migrated to the edge region to be accumulated. As shown in Figure 1C–E, it seems that a few crystals randomly meet to be assembled. Therefore, we cannot rule out that those formed at the center region of crystals are migrated to the edge of the droplet to form a “coffee-ring”.

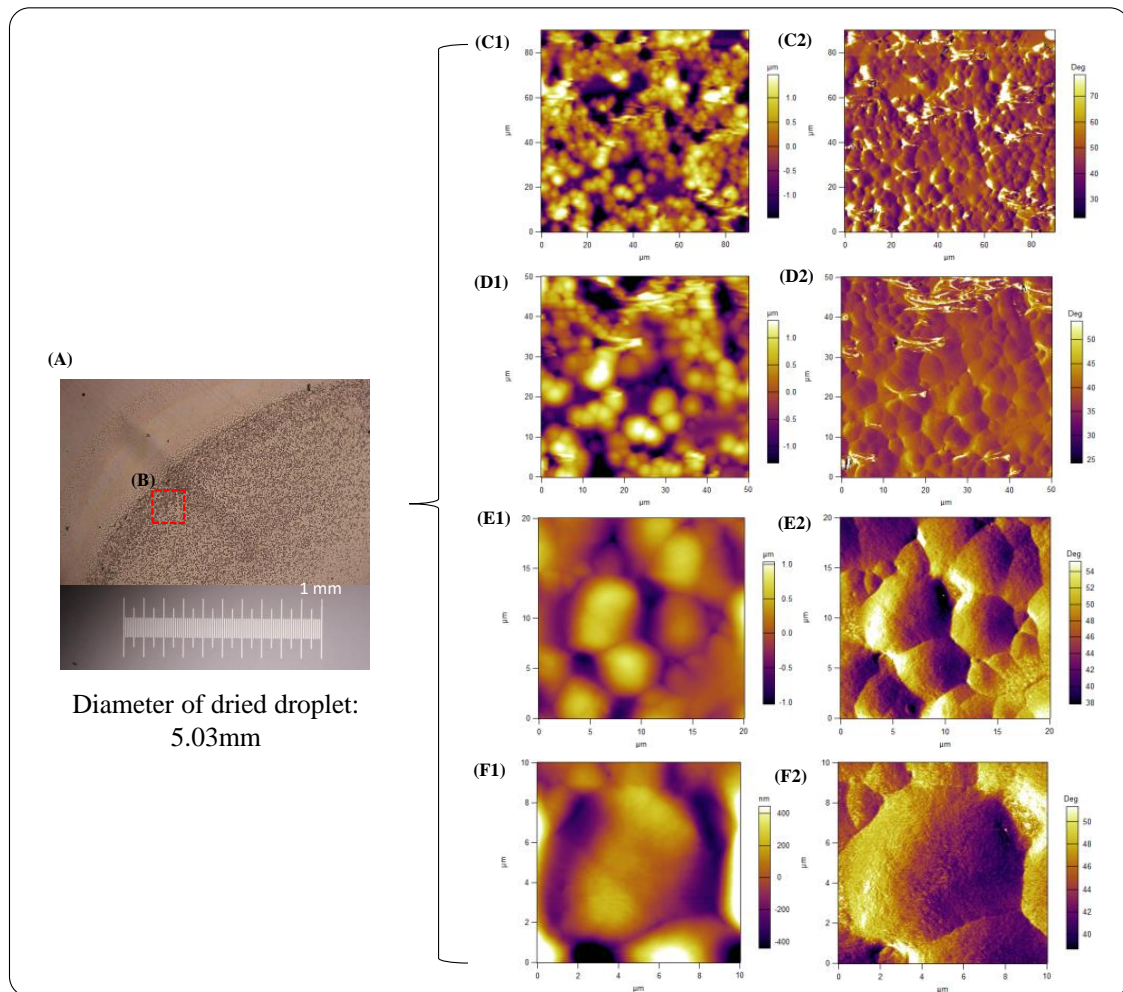


Figure 1. (A) Optical microscopy image of a partially dried PVDF/DMF solution droplet about 5.03 mm in diameter. (B) AFM images of edge region of dried PVDF/DMF solution droplet. (C–F) AFM height and phase images of dried PVDF/DMF droplet. (1) height image, (2) phase images, (C) $90\ \mu\text{m} \times 90\ \mu\text{m}$; (D) $50\ \mu\text{m} \times 50\ \mu\text{m}$; (E) $20\ \mu\text{m} \times 20\ \mu\text{m}$; (F) $10\ \mu\text{m} \times 10\ \mu\text{m}$.

In addition, the size and shape of the PVDF crystals in the edge region are completely different to those in the center region. The crystals in the edge region have a few micrometers in size, and showed polygon-shaped spherulites which have a Mongolian yurt roof-like morphology with a striped surface, which have a Mongolian yurt roof-like morphology with a striped surface, as shown in Figure 1C–F. Additionally, we found that dendritic crystals fill in the gaps of some spherulites boundaries in the center region of the droplet, as shown in Figure 2E,F and Figure 3. The various crystal morphology of PVDF is caused by various crystalline phase. The hill-like-shaped crystals are assigned to the β -form crystal of PVDF [11] and the Mongolian yurt roof-shaped crystals may be assigned to the mixture of β -form or γ -phase crystals [12]. The dendritic-like crystals are assigned to the α -form crystal of PVDF [11]. It means that the nucleation of dendritic-like α -form crystals are developed at the edge of γ -phase spherulites and then are grown to fill in the gaps of the inter-spherulites.

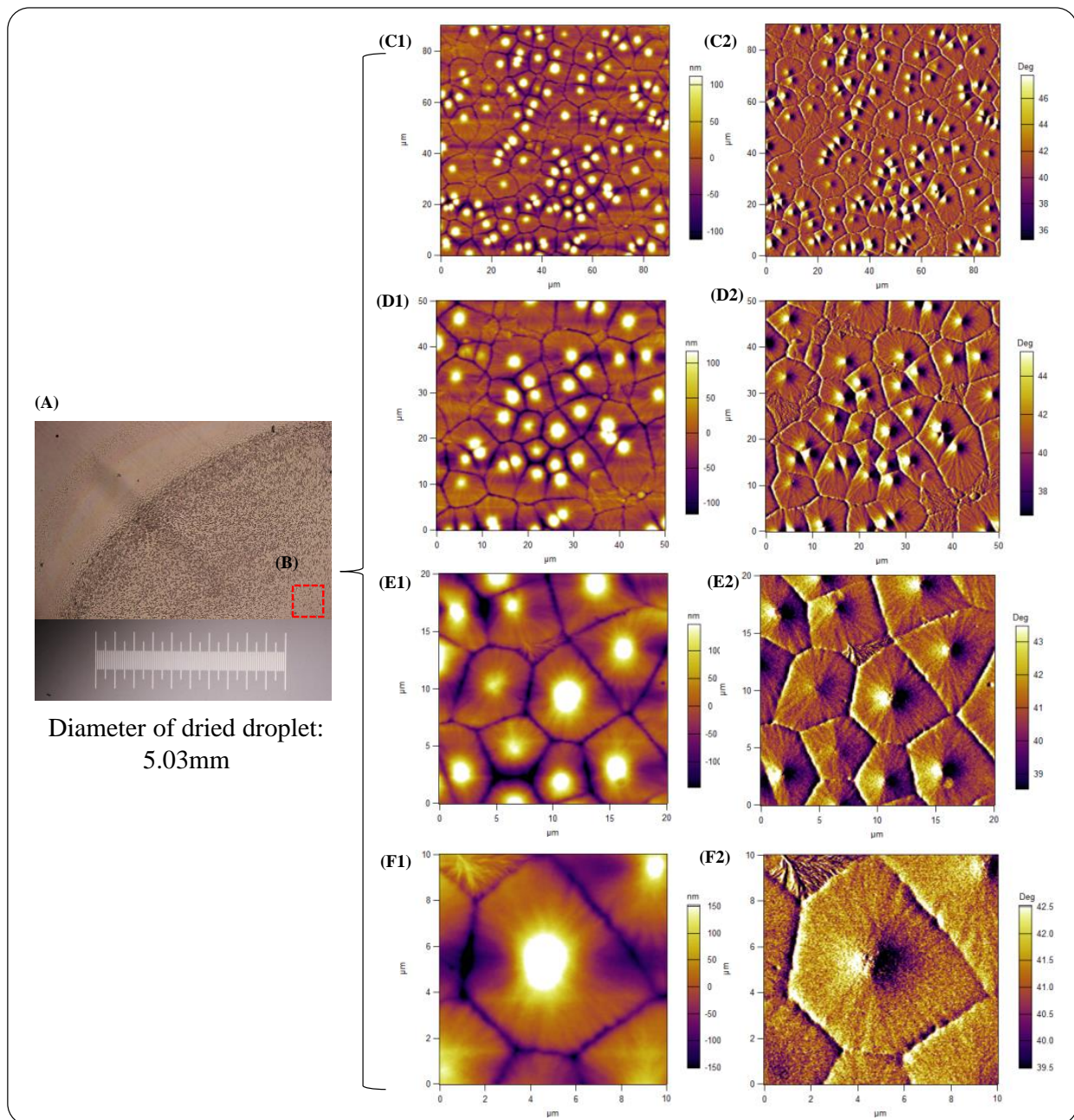


Figure 2. (A) Optical microscopy image of a dried PVDF/DMF solution droplet about 5.03 mm in diameter. (B) AFM images of center region of dried PVDF/DMF solution droplet. (C–F) AFM height and phase images dried PVDF/DMF solution droplet. (1) height image, (2) phase images, (C) 90 $\mu\text{m} \times 90 \mu\text{m}$; (D) 50 $\mu\text{m} \times 50 \mu\text{m}$; (E) 20 $\mu\text{m} \times 20 \mu\text{m}$; (F) 10 $\mu\text{m} \times 10 \mu\text{m}$.

As we know, the β -form crystal has an all *trans* (T) conformation, whereas the α -form crystal has a *trans* (T)-*gauche* (G)-*trans*(T)-*gauche'*(G') (TG₂GT₂G') conformation and the γ phase has a T₃GT₃G' conformation [13,14]. In addition, the evaporation-induced outward capillary flow can induce the shear deformation of polymer coils. Therefore, PVDF β -form nucleation may be promoted by rich *trans* conformers, which are caused by outward capillary flow-induced extended polymer chains. If the time taken to reach a saturated concentration is shorter, the β -form nuclei should be dominated by rich *trans* conformers, whereas if the time taken to reach a saturated concentration is longer, the α -form nuclei should be dominated because the *gauche*-rich conformer-rich state extended chains can be relaxed to a back random coil state before crystallization and the α -form phase nucleation is a kinetically favorable process.

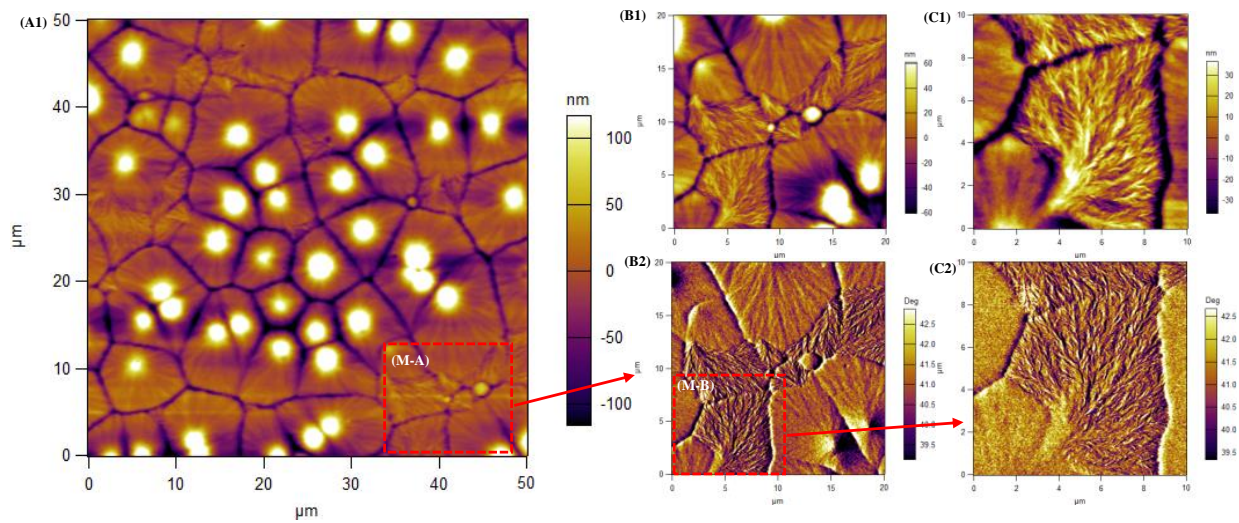


Figure 3. AFM height and phase images of center region of dried PVDF/DMF solution L-droplet. (1) height image, (2) phase image, (A) $50\ \mu\text{m} \times 50\ \mu\text{m}$, (B) $20\ \mu\text{m} \times 20\ \mu\text{m}$, (C) $10\ \mu\text{m} \times 10\ \mu\text{m}$, (M-A) magnified region of (A), (M-B) magnified region of (B).

3.2. Solvent Evaporation Induced Crystal Nucleation and Morphology of PVDF/DMF Solution Small Size Droplet

The diameter of a dried PVDF/DMF solution S-droplet is about $\sim 80\ \mu\text{m}$, as shown in Figure 4A. If we assume the volume of a droplet is mainly determined by the diameter of the dried droplet and the evaporation rate is dependent on the volume of droplet, the solvent evaporation time in the S-droplet should be about 10^4 times fast than that in the L-droplet for the same concentration of solution when the area ratio of the dried small (about $80\ \mu\text{m}$ in diameter) and larger (about $5.02\ \text{mm}$ in diameter) droplets is about 2.53×10^{-4} . As shown in Figures 1 and 4, the “coffee-ring” effect and morphology of dried PVDF/DMF solution S-droplet are different with that of dried PVDF/DMF solution L-droplet. The “coffee-ring” effect in a dried PVDF/DMF solution S-droplet is the size of crystals in the dried PVDF/DMF solution S-droplet are few hundred nanometers more significant than that in a dried PVDF/DMF solution L-droplet. As the size of droplet decreases, the thermal gradient becomes smaller. Accordingly, the Marangoni flow becomes negligible, and the circular evaporation-induced flow transforms into an outward flow [2]. On the other hand, the morphologies of a dried PVDF/DMF solution S-droplet at the edge and center regions are shown in Figure 4D,E, respectively. Aggregated particle-like crystals are presented as clusters in the edge region of the dried PVDF/DMF solution S-droplet, as shown in Figure 4D. In addition, the crystals in the dried PVDF/DMF solution S-droplet the size of crystals in the dried PVDF/DMF solution S-droplet are few hundred nanometers, which is much smaller than that in the dried PVDF/DMF solution L-droplet.

The crystal morphologies of the PVDF/DMF solution S-droplet in the edge and center regions are presented as aggregated particle-like crystals and grain-like crystals, as shown in Figure 4E. Based on the shape of the crystals, we can judge that the α -form crystals are almost absent in the dried PVDF/DMF solution S-droplet. Our previous work showed that the ultrasonic spray-coated PVDF film was almost absent in the α -phase [10].

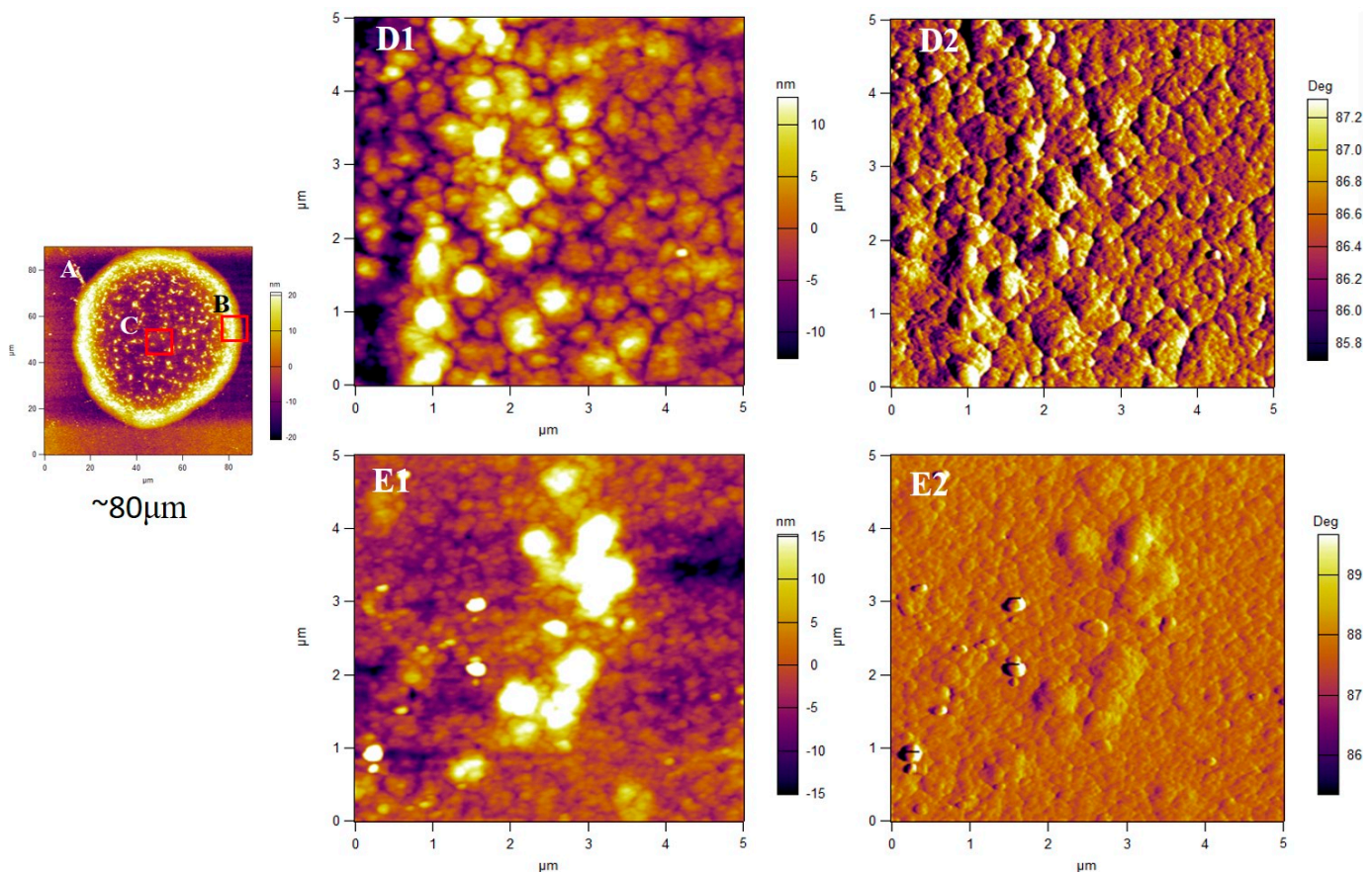


Figure 4. (A) AFM height image of dried PVDF/DMF solution droplet. (B) edge and (C) center regions of dried PVDF/DMF solution S-droplet. (D,E) AFM images of edge and center regions in dried PVDF/DMF solution S-droplet, respectively. (1) height image, (2) phase images, (A) $90\ \mu\text{m} \times 90\ \mu\text{m}$; (D) $5\ \mu\text{m} \times 5\ \mu\text{m}$; (E) $5\ \mu\text{m} \times 5\ \mu\text{m}$.

3.3. Effect of Evaporation Rate on “Coffee-Ring” Formation of Dried Small PVDF Solution Small Size Droplets

To understand the effect of the evaporation rate on outward capillary flow-induced “coffee-ring” formation, we regulated the evaporation rate of the solvent via an increase in the temperature and mixing with the low boiling temperature of the solvent. Since the boiling temperatures of DMF and acetone are 153 and 56 °C, respectively, the evaporation time of DMF/AC (6/4 *v/v*) mixture solvent at RT is shorter than that of DMF at RT. Therefore, the order of evaporation rate of solvents in S-droplets increased as DMF at room temperature (RT) < DMF/AC at RT < DMF at 70 °C. Figure 5A,B show the AFM height images of dried PVDF/DMF solution S-droplets evaporated at RT and 70 °C, respectively. Additionally, Figure 5C shows the AFM height image of a dried PVDF/DMF/AC solution S-droplet evaporated at RT. As shown in Figure 5A–C, the crystal distribution of dried PVDF solution S-droplets at the center region is dependent on the evaporation rate. Among them, the crystals in the center region of the PVDF/DMF solution S-droplet dried at RT showed sparse distribution, whereas the crystals in the center region of the PVDF/DMF solution S-droplet dried at 70 °C showed dense distribution, as shown in Figure 5D. It indicates that the “coffee-ring” formation of dried PVDF solution S-droplets are dependent not only on the evaporation rate but also on the crystallization of PVDF during evaporation.

Why can a fast-enough solvent evaporation rate unexpectedly reduce the “coffee-ring” formation in the case of dried PVDF solution S-droplets? When the concentration of the polymer solution reaches the saturated concentration, the crystal nucleation occurs due to the concentration excess (supersaturation) of the solution above the equilibrium (saturation). The time taken to reach the saturation concentration in the PVDF solution S-droplets becomes shorter as the solvent evaporation rate increases. Additionally, the

polymer chains in the dilute polymer solution S-droplets can be migrated to be edge of droplet or can be deformed by evaporation-induced outward capillary flow. On the other hand, the migrated polymer chains can be further crystallized to form a “coffee-ring” at the edge of the droplet. Accordingly, the migration of polymer chains is promoted by a certain fast solvent evaporation rate; however, it is limited when the evaporation rate is further increased due to solidification.

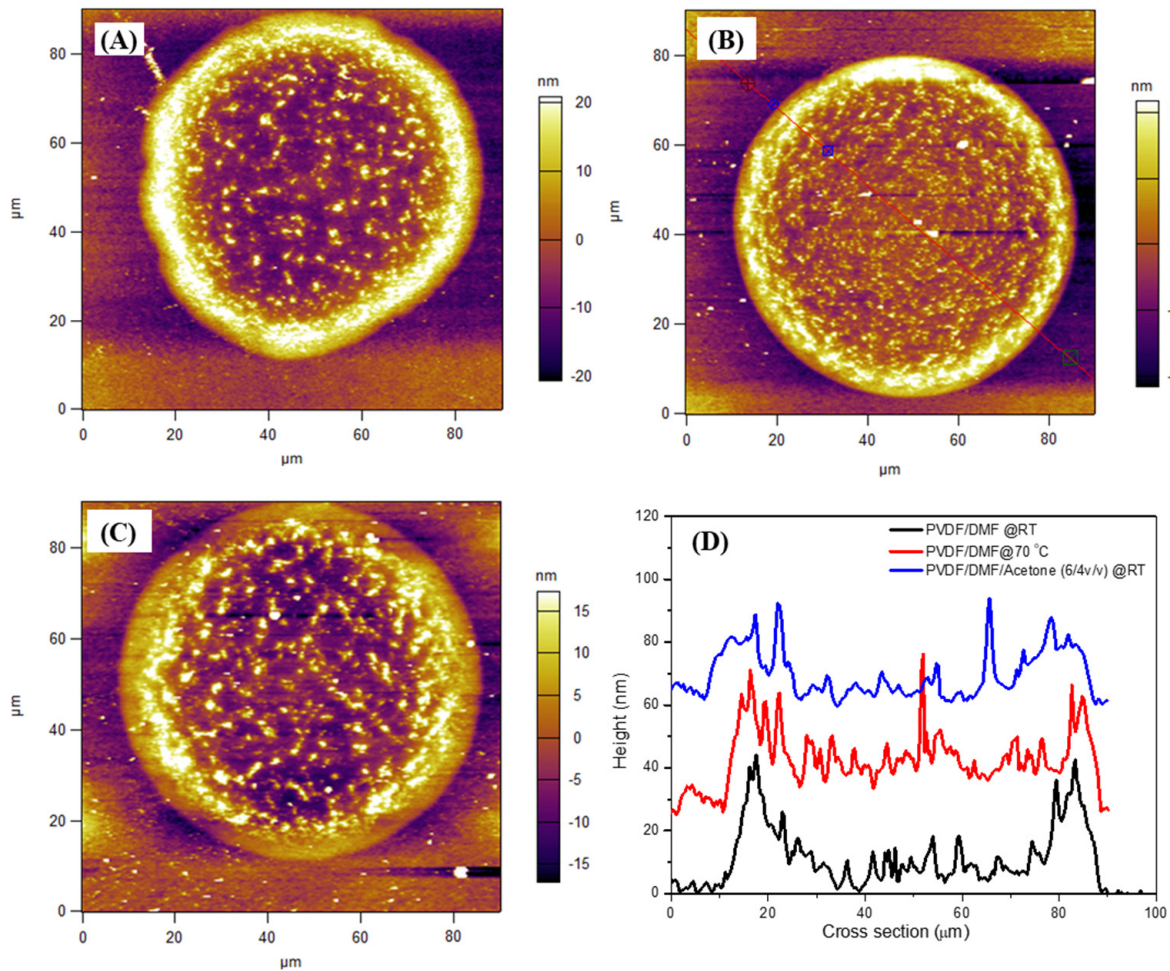


Figure 5. AFM height images of (A) PVDF/DMF solution S-droplets at RT, (B) PVDF/DMF solution S-droplets at 70 °C, (C) PVDF/DMF/acetone solution S-droplets at RT, (D) cross section profiles obtained from AFM images of (A–C).

3.4. Effect of Solution Concentration on “Coffee-Ring” Formation of Dried PVDF/DMF/AC Solution Small-Droplets

To further understand the interplay between the “coffee-ring” effect and crystallization, we investigated the effect of concentration on the “coffee-ring” effect and the crystallization patterns of dried PVDF/DMF/AC solution S-droplets. Figure 6 shows AFM images of dried PVDF/DMF/AC solution S-droplets with various concentrations at RT. As shown in Figure 6, the “coffee-ring” effect of dried PVDF/DMF/AC solution S-droplets weakened as the concentration increased. Additionally, the crystal distribution in the center region of the dried PVDF/DMF/AC solution S-droplets became denser and more uniform as the concentration increased. For example, a scattered distribution of polymer crystals is presented in the dried PVDF/DMF/AC solution S-droplet with an 8 mg/mL concentration, whereas a dense distribution of polymer crystals is presented in the dried PVDF/DMF/AC solution S-droplet with a 20 mg/mL concentration, as shown in Figure 6A,C.

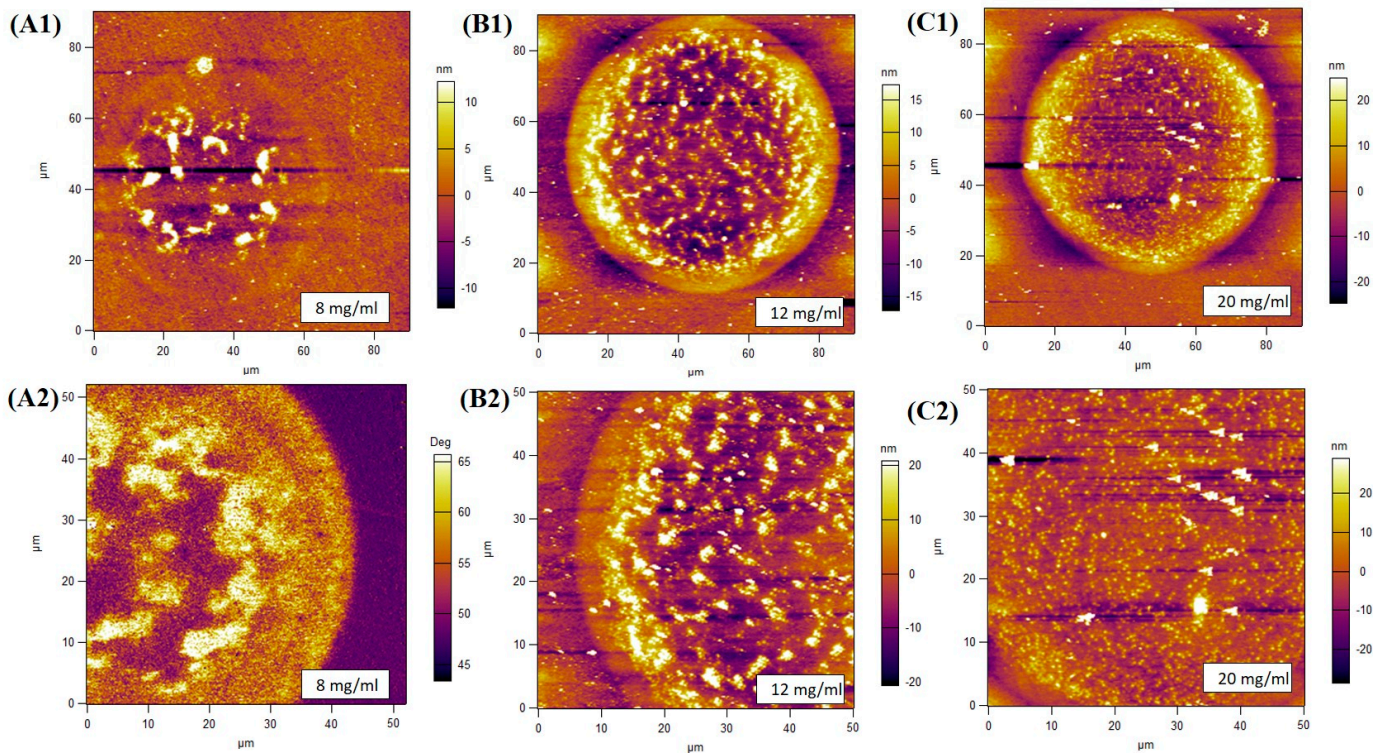


Figure 6. AFM (1) height and (2) phase images of PVDF/DMF/AC solution S-droplets with various concentrations. (A) 8 mg/mL, (B) 12 mg/mL, (C) 20 mg/mL.

If the concentration is low (i.e., 8 mg/mL), the time taken to reach a saturated concentration is longer. Accordingly, the evaporation-induced outward capillary flow can promote the migration of polymer coils, and the deformation and aggregation of the polymer chains are also enhanced before crystal nucleation. On the contrary, if the concentration is high, the time taken to reach a saturated concentration is shorter. In this case, the migration of polymer chains should be restricted by crystal nucleation. Therefore, the “coffee-ring” effect is mainly dominated by the competition between crystal nucleation and the migration of polymer chains. On the other hand, the conformation and entanglement of polymer chains are strongly relative to concentration, which can also influence the migration of chains.

3.5. Effect of Solution Concentration on Polymorphic and Morphology of Ultrasonic Spray-Coated PVDF Films

Based on the results of the structure and morphology formation of dried PVDF solution S-droplets, we can conclude that the evaporation of an S-droplet benefits from obtaining a submicron size β -form phase, even though the “coffee-ring” effect occurs. However, the structure and morphology of PVDF films formed by S-droplets’ deposition during the USC process may be different within the case of S-droplet evaporation. In this case of film formation, the solvent evaporation and amalgamation of S-droplets may have simultaneously taken place. The crystal structure and morphology of spray-coated PVDF films with various films were characterized using FTIR, AFM and 2D GIWAXS methods, as shown in Figures 7 and 8, respectively. In Figure 7A, the bands at 614, 766, 795, 975 and 1402 cm^{-1} are sensitive to the α -phase, and the bands at 840 and 1278 cm^{-1} are sensitive to the β -phase [14]. In addition, the band at 1234 cm^{-1} can be assigned to the γ -form phase [14]. As shown in Figure 7A, the bands at 976, 763, and 612 cm^{-1} are evidently observed in the PVDF films, except for the PVDF film with a 12 mg/mL concentration. It means that the α -form phase exists in the films except for the PVDF film with a 12 mg/mL concentration. In addition, the intense absorbance of the band at 1234 cm^{-1} is shown in all the films, indicating the co-existence of a certain amount of the γ -form phase.

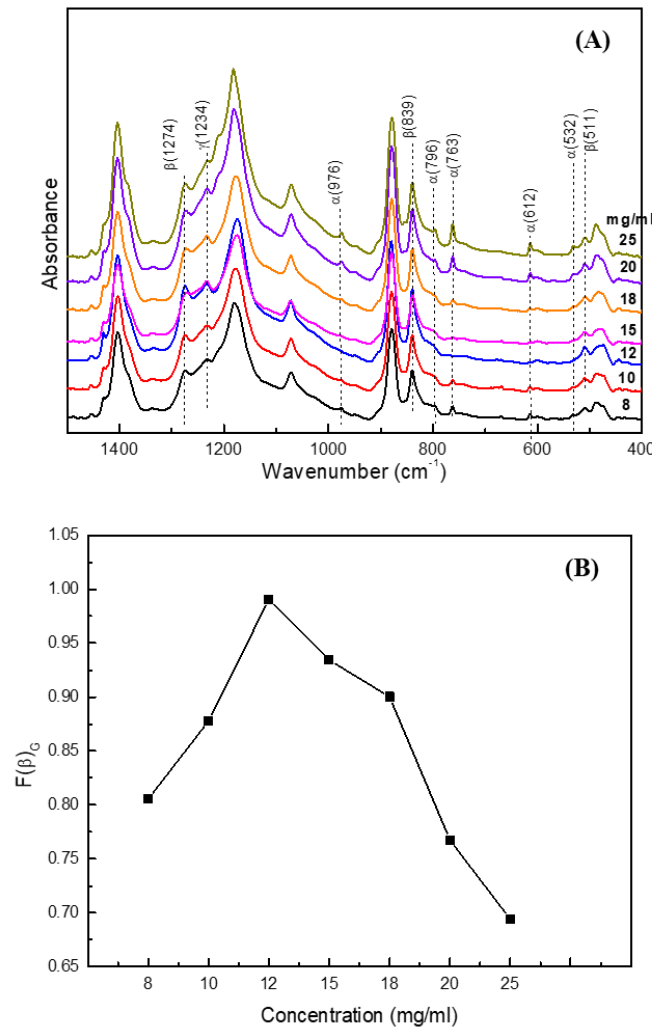


Figure 7. (A) FTIR spectra of ultrasonic spray-coated PVDF films and (B) the solution concentration-dependent relative fraction of β -form crystal ($F(\beta)_G$).

The relative ratio of the α - and β -phases can be estimated by the absorbances of characteristic bands of α - and β -phases. Gregorio et al. [15] suggested that the relative β -phase content ($F(\beta)_G$) can be determined by $F(\beta)_G = \frac{A_{840}}{\left(\frac{K_{840}}{K_{766}}\right)A_{766} + A_{840}}$, where A_{766} and A_{840} refer to the absorbances at 766 and 840 cm^{-1} ; and K_{766} ($6.1 \times 10^4 \text{ cm}^2 \text{ mol}^{-1}$) and K_{840} ($7.7 \times 10^4 \text{ cm}^2 \text{ mol}^{-1}$) are the absorption coefficients of 766 and 840 cm^{-1} , respectively. Those at 766 and 840 cm^{-1} are sensitive to the α - and β -phases, respectively. However, some researchers argue that the absorbance peak at 840 cm^{-1} is attributed to both β - and γ -phases. Benz et al. [16] suggests that the relative β -phase content can be calculated based on the absorbance of the bands at 762 and 1272 cm^{-1} as $F(\beta)_B = \frac{A_{1272}}{\left(\frac{K_{1272}}{K_{762}}\right)A_{762} + A_{1272}}$, where A_{762} and A_{1272} are the absorbance of the bands at 762 and 1272 cm^{-1} , respectively; and K_{762} ($0.365 \mu\text{m}^{-1}$) and K_{1272} ($0.14 \mu\text{m}^{-1}$) are the absorption coefficients of the bands at 762 and 1272 cm^{-1} , respectively. Those at 762 and 1272 cm^{-1} are sensitive to the α - and β -phases, respectively. Our calculated results showed that the calculated relative fraction of the β -phase using both methods is similar. Therefore, we adopted the method suggested by Gregorio et al. to calculate the relative fraction of the β -form phase in this work. Figure 7B shows the $F(\beta)_G$ of spray-coated PVDF films prepared by various concentrations. The $F(\beta)_G$ of the spray-coated PVDF films increases as the concentration increases up to

12 mg/mL, and then decreases as the concentration increases. For example, the $F(\beta)_G$ of PVDF films with 8, 12 and 20 mg/mL concentrations are 0.80, 0.99 and 0.69, respectively. However, the absolute crystallinity of the α -, β -, and γ -phases are hard to obtain using FTIR analysis based on the literature-provided absorption coefficients, because the calculation of absorbance is strongly dependent on the criterion of local baseline.

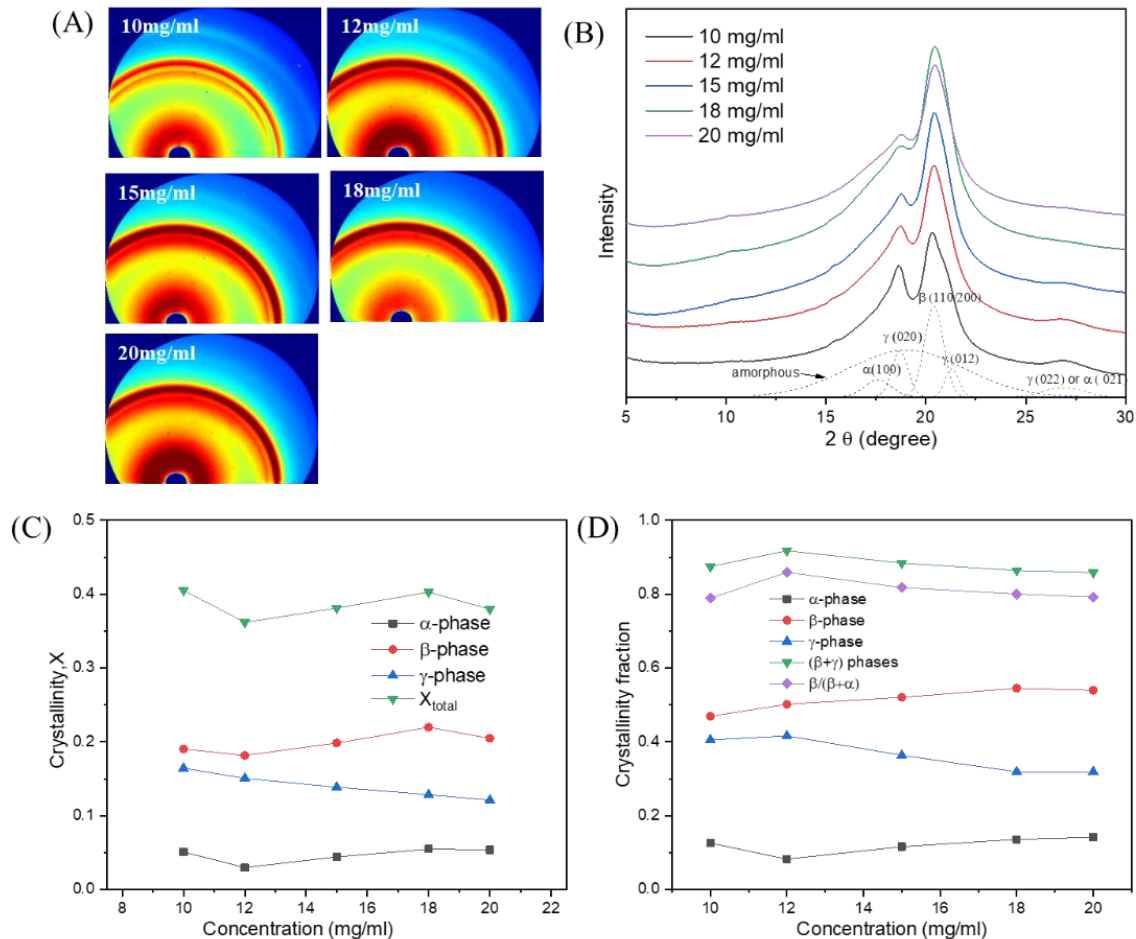


Figure 8. (A) 2D GIWAXS patterns of ultrasonic spray-coated PVDF films obtained by various concentrations. (B) 1D GIWAXS profiles of ultrasonic spray-coated PVDF films obtained by various concentrations. (C) Concentration-dependent crystallinity of various crystalline phases of ultrasonic spray-coated PVDF films. (D) Concentration-dependent crystallinity fractions of a certain crystalline phase in the crystallinity of ultrasonic spray-coated PVDF films.

In order to more clearly identify the crystalline phase, we observed the 2D GIWAXS patterns as shown in Figure 8A. The 2D GIWAXS patterns of the PVDF films showed that the crystals did not show an obvious orientation. In the 1D GIWAXS profile of the PVDF films (Figure 8B), the relative intensities of the diffraction peaks at 18.7° and 21.3° obviously reduced as the concentration increased. The peaks at $2\theta = 18.7^\circ$ and 21.3° can be attributed to the diffraction of the (020) and (012) of the γ -phase, respectively. Additionally, the weak diffraction peak at around $2\theta = 26.8^\circ$ is attributed to the diffraction of the (021) plane of α -phase or (022) plane of the γ -phase. It indicates that the relative γ -phase content decreases as the concentration increases. The weak shoulder diffraction peak at $2\theta = 17.6^\circ$ is attributed to the diffraction of the (100) plane of α -phase, and the diffraction peak at $2\theta = 20.4^\circ$ is attributed to the diffraction of the (1 1 0)/(2 0 0) planes of the β -phase.

To quantitatively analyze the crystallinity of each phase, the individual diffraction peak areas were obtained using the peak fitting method. The crystallinity of the α -, β - and γ -phases in PVDF films are shown Figure 8C. The GIWAXS results showed that the

total crystallinity of the PVDF films is about 0.42, which is almost independent of the concentration. However, the crystallinity of the α - and β -phases slightly increased as the concentration increased, whereas the crystallinity of γ -phase slightly decreased as the concentration increased. The crystallinity fractions of the α -, β - and γ -phases in the PVDF film with a 12 mg/mL concentration are 0.08, 0.50 and 0.42, respectively. Therefore, the β and γ -phases are the dominate crystalline phases in the PVDF films. This means that the S-droplets evaporation-induced rich T conformer still play important roles in the nucleation of β - and γ -phases in the case of spray-coated films. The crystallinity fractions of electroactive phases (β and γ) and β -phase in α - and β -phases have similar concentration-dependent trends and showed the highest values at a 12 mg/mL concentration, as shown in Figure 8D. The trend of the concentration-dependent crystallinity fractions of β -phase in α - and β -phases by GIWAXS is similar to that obtained using FTIR.

Figure 9 shows the AFM amplitude and phase images of PVDF films with 10, 12 and 20 mg/mL concentrations. The spherulite crystal morphology of PVDF is attributed to α -phase crystals, and the particle-like crystal morphology of PVDF is attributed to β - or γ -phase crystals. In contrast with the PVDF film with a 12 mg/mL concentration, some spherulite crystals are observed in the AFM images of PVDF films with 10 and 20 mg/mL concentrations.

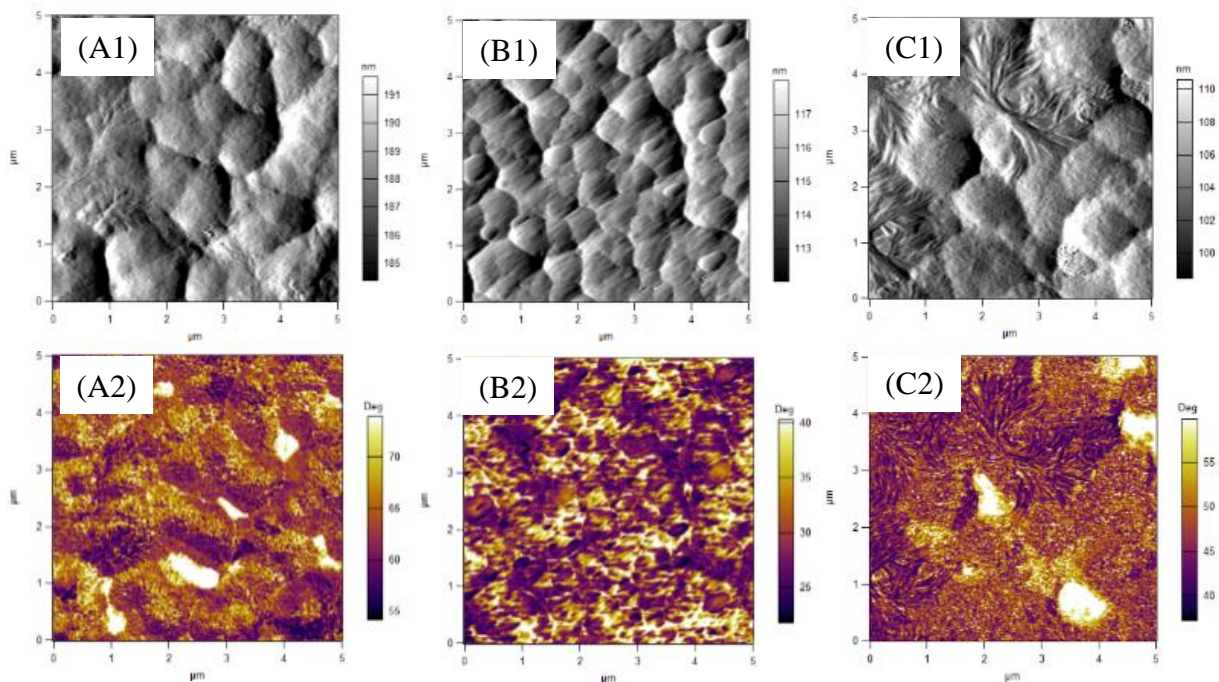


Figure 9. AFM (1) amplitude and (2) phase images of dried PVDF/DMF/acetone solution droplets with various concentrations. (A) 10 mg/mL, (B) 12 mg/mL, (C) 20 mg/mL.

4. Discussion

It is generally recognized that the low evaporation rate is favorable to the nucleation and growth of the thermodynamically stable β -form phase, whereas a high evaporation rate yields the kinetically favorable metastable α -form phase in the case of solvent casting [17,18]. In addition, the PVDF β -phase is strongly dependent on solution type [19,20], temperature [15] and solvent evaporation rate [18], etc. For example, Gregorio [11] suggested that the crystallization of PVDF from solution at a temperature $T < 70$ °C always predominantly results in the β -phase of PVDF, regardless of the solvent used, as long as it is a good solvent for PVDF. As the temperature increases, α -phase formation increases, becoming predominant at $T > 110$ °C. Ma et al. [21] investigated the effect of mixed solvents on the crystallization of PVDF. Their results showed that the crystallization of PVDF from tetrahydrofuran (THF)/N,N-dimethylformamide (DMF) mixed solvents yielded the α -

and β -form phases, and the β -form phase content was proportional to the DMF content. Zhao et al. [22] also investigated the crystallization of PVDF from the DMF/ethanol mixed solvent nonsolvent. They found that the low ethanol content favored the formation of β -form phase, while the high ethanol content resulted predominantly in the α -form phase. Gregorio et al. [18] investigated the effect of solvent evaporation rate on the crystalline phase of solvent-cast PVDF films. They suggested that the low evaporation rate favors the nucleation and growth of the thermodynamically stable β -form phase, whereas high evaporation rates yield the kinetically favorable metastable α phase. When the PVDF concentration increases during the process and growth takes place, the nuclei are already in the phase determined by the initial evaporation rate. They argued that the competition in the formation of the α - and β -form phases does not occur during the whole crystallization process, as the distinct, constant evaporation rates during nucleation are important for leading to different relative amounts of the crystalline phases. Horibe et al. [17] also investigated the relationship between the PVDF crystalline structure and the solvent evaporation rate. They prepared spin-coated PVDF films with various solvents and the solvent evaporation rate was quantified by measuring the sample weight with an electronic balance. Their results indicated that the crystalline structures of forms I (β -form), II (α -form) and III (γ -form) of PVDF were obtained when the solvent evaporation rates were <0.0001 , >0.2 and between 0.03 and $0.00058 \text{ g min}^{-1}$, respectively. Recently, Nishiyama et al. [20] investigated the effect of the solvent evaporation rate and solvent type on the crystal formation of PVDF prepared using the spin-coating method. Their results showed that the crystalline phase of PVDF changed in the order of α -, γ - and β -form with the increasing dipole moment of the solvent in the much-solvent-remaining state, and the crystalline structure of PVDF with a higher dipole moment of solvents (hexamethyl phosphor amide) was dominantly dependent on the evaporation rate in the almost all solvent evaporated states, and varied in the order of β -, γ - and α -form with the increasing solvent evaporation rate. However, the PVDF with a lower dipole moment of solvents (triethyl phosphate) always formed α -form phase, regardless of the evaporation rate.

However, the crystallization of a PVDF solution in the droplets is different with that in the casting or spin coating due to the evaporation-induced flows occurring. In the case of droplets, the migration and shear deformation of polymer chains generally occur during solvent evaporation. The solvent evaporation-induced outward capillary flow can induce the migration of chains and the shear deformation of polymer chains to cause the conformational transition of *gauche* to *trans*. Therefore, the nucleation of PVDF β - and γ -phases are promoted by droplet evaporation at the near boundary of the droplet, as shown in Figure 10. Additionally, the crystal growth of PVDF is strongly restricted by the evaporation-induced solidification. The “coffee-ring” effect of dried PVDF droplets was mainly caused by accumulated crystal nucleation at the edge region of the droplet, which was enhanced by migrated polymer chains. The slow solidification of droplets can promote α -form phase nucleation because the *trans* conformers can be transformed to *gauche* conformers by relaxation and the α -form phase is kinetically favorable. The fast solvent evaporation can strongly restrict the crystal growth, resulting in the formation of crystals of a submicron size. In addition, the formation of the “coffee-ring” in the S-droplets is strongly influenced by the droplet size, solvent evaporation rate and concentration. Accordingly, the final crystal structure and morphology of the dried PVDF S-droplets and spray-coated PVDF films are determined by the interplay between the evaporation-induced migration of polymer chains, crystallization and solidification.

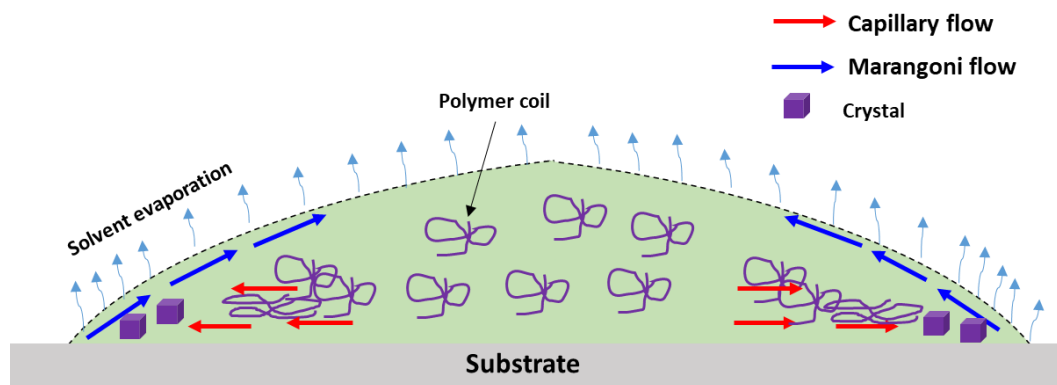


Figure 10. Schematic illustration of solvent evaporation-induced flows and crystallization of PVDF droplet during solvent evaporation.

5. Conclusions

In this work, we investigated the effect of droplet size, solvent evaporation rate and concentration on the “coffee-ring” effect, crystal structure and morphology of dried PVDF solution droplets. The crystal morphology and crystal distribution of dried PVDF droplets in the center and edge regions were different due to the “coffee-ring” effect. The “coffee-ring” effect of dried PVDF droplets was mainly composed of accumulated crystals at the edge region of the droplet, which was mainly made by the crystallization of migrated chains. The “coffee-ring” effect of PVDF droplets was dependent on the droplet size, solvent evaporation rate and concentration, which was determined by an interplay between the migration of chains and solidification. In addition, the nucleation of PVDF β - or γ -phase was promoted by fast solvent evaporation-induced outward capillary flow and the crystal growth was significantly restricted by fast solidification in the case of droplet evaporation. Our results showed that the sub-millimeter size droplets can be obtained using the ultrasonic spray-coating method, and decreasing the droplet size and controlling the solvent evaporation were effective ways to improve the electroactive crystalline phases’ (β - and γ -phases) content and decrease the crystal size of PVDF.

Author Contributions: Conceptualization, writing—review and editing, project administration, and funding acquisition, Y.L.; validation, data curation, investigation, original draft preparation, S.W. All authors have read and agreed to the published version of the manuscript.

Funding: This research was funded by Natural Science Foundation of Beijing Municipality, China, grant number 2172023.

Data Availability Statement: Not Applicable.

Acknowledgments: This research work was supported by Natural Science Foundation of Beijing Municipality (2172023). The 2D GIWAXS experiments were supported by Beijing Synchrotron Radiation Facility (BSRF) in Beijing, China.

Conflicts of Interest: The authors declare no conflict of interest.

References

1. Diao, Y.; Shaw, L.; Bao, Z.; Mannsfeld, S.C.B. Morphology control strategies for solution-processed organic semiconductor thin films. *Energy Env. Sci.* **2014**, *7*, 2145–2159. [[CrossRef](#)]
2. Zang, D.; Tarafdar, S.; Tarasevich, Y.Y.; Dutta Choudhury, M.; Dutta, T. Evaporation of a Droplet: From physics to applications. *Phys. Rep.* **2019**, *804*, 1–56. [[CrossRef](#)]
3. Deegan, R.D.; Bakajin, O.; Dupont, T.F.; Huber, G.; Nagel, S.R.; Witten, T.A. Capillaryflowasthecause of ring stains fromdried liquid drops. *Nature* **1997**, *389*, 827–829. [[CrossRef](#)]
4. Zhou, J.; Man, X.; Jiang, Y.; Doi, M. Structure Formation in Soft-Matter Solutions Induced by Solvent Evaporation. *Adv. Mater.* **2017**, *29*, 1703769. [[CrossRef](#)]

5. Deegan, R.D.; Bakajin, O.; Dupont, T.F.; Huber, G.; Nagel, S.R.; Witten, T.A. Contact line deposits in an evaporating drop. *Phys. Rev. E* **2000**, *62*, 756–765. [[CrossRef](#)]
6. Yu, X.; Xing, R.; Peng, Z.; Lin, Y.; Du, Z.; Ding, J.; Wang, L.; Han, Y. To inhibit coffee ring effect in inkjet printing of light-emitting polymer films by decreasing capillary force. *Chin. Chem. Lett.* **2019**, *30*, 135–138. [[CrossRef](#)]
7. Mampallil, D.; Eral, H.B. A review on suppression and utilization of the coffee-ring effect. *Adv. Colloid Interface Sci.* **2018**, *252*, 38–54. [[CrossRef](#)]
8. Hu, Y.; Zhang, X.; Qiu, M.; Wei, Y.; Zhou, Q.; Huang, D. From coffee ring to spherulites ring of poly(ethylene oxide) film from drying droplet. *Appl. Surf. Sci.* **2018**, *434*, 626–632. [[CrossRef](#)]
9. Rietveld, I.B.; Kobayashi, K.; Yamada, H.; Matsushige, K. Morphology control of poly(vinylidene fluoride) thin film made with electrospray. *J. Colloid Interface Sci.* **2006**, *298*, 639–651. [[CrossRef](#)]
10. Wang, S.; Liang, Y. Transparent and ferroelectric poly(vinylidene fluoride) film achieved by simple ultrasonic spray coating method. *Mater. Lett.* **2019**, *247*, 71–74. [[CrossRef](#)]
11. Gregorio, R. Determination of the α , β , and γ crystalline phases of poly(vinylidene fluoride) films prepared at different conditions. *J. Appl. Polym. Sci.* **2006**, *100*, 3272–3279. [[CrossRef](#)]
12. Kang, S.J.; Park, Y.J.; Sung, J.; Jo, P.S.; Park, C.; Kim, K.J.; Cho, B.O. Spin cast ferroelectric beta poly(vinylidene fluoride) thin films via rapid thermal annealing. *Appl. Phys. Lett.* **2008**, *92*, 012921. [[CrossRef](#)]
13. Lovinger, A.J. Ferroelectric Polymers. *Science* **1983**, *220*, 1115–1121. [[CrossRef](#)]
14. Martins, P.; Lopes, A.C.; Lanceros-Mendez, S. Electroactive phases of poly(vinylidene fluoride): Determination, processing and applications. *Prog. Polym. Sci.* **2014**, *39*, 683–706. [[CrossRef](#)]
15. Rinaldo Gregorio, J.; Cestari, M. Effect of crystallization temperature on the crystalline phase content and morphology of poly(vinylidene fluoride). *J. Polym. Sci. Part B Polym. Phys.* **1994**, *32*, 859–870. [[CrossRef](#)]
16. Benz, M.; Euler, W.B. Determination of the Crystalline Phases of Poly(vinylidene fluoride) Under Different Preparation Conditions Using Differential Scanning Calorimetry and Infrared Spectroscopy. *J. Appl. Polym. Sci.* **2003**, *89*, 1093–1100. [[CrossRef](#)]
17. Horibe, H.; Sasaki, Y.; Oshiro, H.; Hosokawa, Y.; Kono, A.; Takahashi, S.; Nishiyama, T. Quantification of the solvent evaporation rate during the production of three PVDF crystalline structure types by solvent casting. *Polym. J.* **2004**, *46*, 104–110. [[CrossRef](#)]
18. Chinaglia, D.L.; Gregorio, R., Jr.; Stefanello, J.C.; Altafim, R.A.P.; Wirges, W.; Wang, F.; Gerhard, R. Influence of the solvent evaporation rate on the crystalline phases of solution-cast poly(vinylidene fluoride) films. *J. Appl. Polym. Sci.* **2010**, *116*, 785–791. [[CrossRef](#)]
19. Park, Y.J.; Kang, Y.S.; Park, C. Micropatterning of semicrystalline poly(vinylidene fluoride) (PVDF) solutions. *Eur. Polym. J.* **2005**, *41*, 1002–1012. [[CrossRef](#)]
20. Nishiyama, T.; Sumihara, T.; Sato, E.; Horibe, H. Effect of solvents on the crystal formation of poly(vinylidene fluoride) film prepared by a spin-coating process. *Polym. J.* **2016**, *49*, 1–7. [[CrossRef](#)]
21. Ma, W.; Zhang, J.; Chen, S.; Wang, X. Crystalline Phase Formation of Poly(vinylidene fluoride) from Tetrahydrofuran/N,N-dimethylformamide Mixed Solutions. *J. Macromol. Sci. Part B Phys.* **2008**, *47*, 434–449. [[CrossRef](#)]
22. Zhao, X.; Cheng, J.; Chen, S.; Zhang, J.; Wang, X. Controlled Crystallization of Poly(vinylidene fluoride) Chains from Mixed Solvents Composed of Its Good Solvent and Nonsolvent. *J. Polym. Sci. Part B Polym. Phys.* **2010**, *48*, 575–581. [[CrossRef](#)]